ACS APPLIED MATERIALS & INTERFACES

Research Article

www.acsami.org

Microwave-Assisted Fabrication of Nanoparticulate TiO_2 Microspheres for Synergistic Photocatalytic Removal of Cr(VI) and Methyl Orange

Yong Yang,[†] Guozhong Wang,*[,†] Quan Deng,[†] Dickon H. L. Ng,[‡] and Huijun Zhao[†,§]

[†]Key Laboratory of Materials Physics, Centre for Environmental and Energy Nanomaterials, Anhui Key Laboratory of Nanomaterials and Nanotechnology, Institute of Solid State Physics, Chinese Academy of Sciences, P.O. Box 1129, Hefei 230031, P.R. China

[‡]Department of Physics, The Chinese University of Hong Kong, Shatin, New Territory, Hong Kong

[§]Centre for Clean Environment and Energy, Gold Coast Campus, Griffith University, Queensland 4222, Australia

Supporting Information

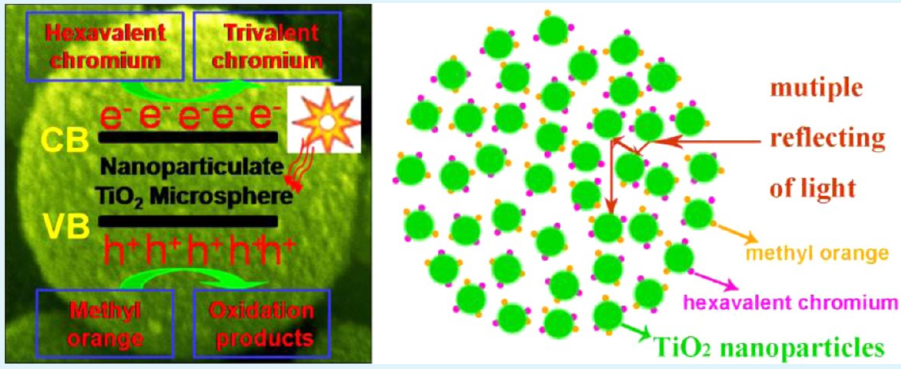

ABSTRACT: High yield production of micro/nanostructured nanoparticulate TiO_2 microspheres (NTMs) via a facile microwave-assisted hydrothermal approach was investigated. The rapid and uniform microwave heating could reduce the reaction time to 30 min, an order of magnitude shorter than that of conventional hydrothermal methods. The characterization data confirmed that the resultant NTMs were highly uniform in size, having an average diameter of ~0.5 μm. The obtained NTMs were found to be constructed by well-crystallized anatase phase nanoparticles ranging from 5 to 10 nm that can be readily controlled by the microwave radiation temperature. Nitrogen sorption isotherm analysis revealed that the obtained NTMs possessed abundant mesoporous structures with a high specific surface area of 124 $m^2\ g^{-1}$. An in situ self-aggregation formation process under controllable pH in presence of urea was proposed. The results obtained from the application of NTMs for simultaneous photocatalytic decontamination of Cr(VI) and methyl orange (MO) demonstrated a strong synergistic effect that dramatically enhanced both Cr(VI) reduction and MO oxidation removal efficiencies. This work not only enriched the synthesis methods of the micro/nanostructured TiO_2, but also provided a new means to improve the photocatalytic efficiency via structural-induced synergistic effect, applicable to the other catalysis systems.

KEYWORDS: *microwave, TiO_2, synergistic, photocatalytic, Cr(VI), methyl orange*

1. INTRODUCTION

Industrial processes, such as electroplating, paint making, leather tanning, and others, have made hexavalent chromium (Cr(VI)) to be a widespread pollutant in wastewaters.[1,2] A general way to reduce the toxicity of Cr(VI) is to convert Cr(VI) into a low toxic trivalent chromium (Cr(III)), which can be removed through the precipitation or adsorption processes. Heterogeneous photocatalysis with semiconductor mediated redox reactions have been proven to be effective for detoxification of harmful pollutants in wastewaters.[3−5] On one hand, extensive efforts have been made to achieve effective and efficient photocatalytic reduction removal of Cr(VI).[6,7] On the other hand, the application of photocatalysis to oxidative degrade industrial dyes in wastewaters is a well-known process.[8−10] However, vast majority of reported works have investigated the photocatalytic reduction removal of Cr(VI) or oxidative degradation of dyes alone, while little attention is paid to collectively treat the samples containing both Cr(VI) and dyes.[3,4] In fact, Cr(VI) and dyes often coexist in many wastewaters. Therefore, the study of their mutual interactions in photocatalytic conversion processes is of important for the practical use of heterogeneous photocatalysis.

Several research groups have studied the simultaneous decontamination of Cr(VI) and dyes using the nano-sized

Received: December 5, 2013
Accepted: January 15, 2014
Published: January 15, 2014

TiO_2 photocatalyst.[3,4,11−13] The studies indicated that when Cr(VI) and dyes were coexisted in a sample, the obtained Cr(VI) reduction and dye oxidation efficiencies were found to be higher than that of samples containing Cr(VI) or dyes alone, suggesting a synergistically enhanced phenomenon.[4,11−13] Nevertheless, there were also studies showing that the rates of Cr(VI) reduction and dye oxidation in the ternary catalytic systems of TiO_2/Cr(VI)/dye were lower than those of the respective binary systems (TiO_2/Cr(VI) and TiO_2/dye), due partially to the deactivation of the nano-sized TiO_2 catalysts.[3] Besides, commonly used nano-sized TiO_2 powders such as Degussa P25 tend to aggregate during liquid phase photocatalysis, resulting in a undesirable reduction in the photocatalytic activity. Additionally, the nano-sized catalysts are difficult to be recovered after use, even with the assistance of the high-speed centrifugation. Recently, hierarchical micro/nanostructures with high surface areas and abundant mesoporous structures have stimulated much attention since such structures embrace the high dispersion and easy recovery features of micrometer-sized structures, and large surface area and high activity of nano-sized structures.[14−16] They are the micrometer-size materials but assembled with reactive low-dimensional nano-sized building blocks (such as nanoparticles, nanowires, nanotubes, and nanosheets). It has been demonstrated that the micro/nanostructures exhibited unique properties differing remarkably from those of the mono-morphological micrometer- or nanosized structures.[14−16] It was reported that the hierarchically micro/nanostructured nanoporous TiO_2 hollow spheres exhibited enhanced photocatalytic activity when compared to commercial Degussa P25 TiO_2 powders for the photocatalytic degradation of dye solution.[17] It is expected that TiO_2 in the form of micro/nanostructure would be more favorable to show its effective activity in the simultaneous decontamination of Cr(VI) and dyes compared to nanosized TiO_2. However, there is no report regarding the simultaneous decontamination of Cr(VI) and dyes using the hierarchical micro/nanostructured TiO_2 photocatalyst.

Over the past few years, huge efforts have been made to fabricate hierarchical micro/nanostructured TiO_2 such as organic/inorganic template methods, hydrothermal methods and solve-thermal methods.[17−23] For example, Yu et al. have reported the fabrication of hierarchical micro/nanostructured nanoporous TiO_2 hollow microspheres by using SiO_2 microspheres as templates and TiF_4 as the precursor.[17] Yang et al. have reported a two-step method for the fabrication of micro/nanostructured TiO_2 microspheres,[19] including the formation of amorphous titanium diglycolate microspheres first and then the hydrothermal transformation of the amorphous titanium diglycolate microspheres into anatase phase of TiO_2 at 180 °C for 6 h. However, most of these methods involved tedious and time consuming procedures, and required the use of expensive and toxic precursors such as TiF_4, greatly limiting the widespread applications of such materials. From synthetic viewpoint, facile, and rapid fabrication of large quantity of high quality micro/nanostructured TiO_2 remains a great challenge because of the complicity involved.

In the present work, we demonstrated the synthesis of micro/nanostructured NTMs with a high yield via a single-step microwave-assisted hydrothermal method. Titanium sulfate and urea were used as the precursor, which were inexpensive and nontoxic. The reaction time was as short as 30 min. The photocatalytic activities of the resultant NTMs were evaluated by photocatalytic detoxification of Cr(VI) and degradation of MO. The strong synergistic effect was demonstrated by simultaneous decontamination of Cr(VI) and MO.

2. EXPERIMENTAL SECTION

2.1. Fabrication. All reagents were commercially supplied and used without further purification. Titanium sulfate ($Ti(SO_4)_2$, ≥96.0%, Shanghai Nanhui Chemical Reagent Co. Ltd, CP) and urea ($CO(NH_2)_2$, ≥99.0%, Guoyao Chemical Reagent Co. Ltd, AR) were chosen as raw materials. Deionized water was used in all experiments. In a typical preparation procedure, 2.0 mmol of $Ti(SO_4)_2$ and 4.0 mmol of $CO(NH_2)_2$ were added to 40 mL of deionized water. After continuous stirring for 3 h, the mixed suspension was transferred into a 100 mL Teflon-lined autoclave, which was heated at 180 °C for 30 min under microwave irradiation (heating rate was about 20 °C/min) (QWAVE 4000, 2450 MHz, up to 1200 W, Questron Technologies Corp). After cooled to room temperature, the white precipitates were collected, washed with deionized water followed by rinsing with ethanol and dried in an oven at 70 °C for 5 h.

2.2. Characterization. The phases of the products were identified by X-ray diffraction analysis (XRD, Philips X'pert PRO) using Ni-filtered monochromatic CuKα radiation at 40 keV and 40 mA. The morphology and structure of the product were characterized by field emission scanning electron microscope (FESEM, Sirion 200 FEI) using an accelerating voltage of 5 kV, and transmission electron microscopy (TEM, JEOL-2010, 200 kV) with an energy dispersive X-ray spectrometer (EDX, Oxford, Link ISIS). The powders were ultrasonically-dispersed in ethanol. Then the suspensions were dropped onto the SEM stub and holey-carbon grid for SEM and TEM examination respectively. The specific surface area of the samples was determined by nitrogen adsorption (Micrometrics ASAP 2020M) at 77 k using the Brunauer−Emmett−Teller (BET) equation. X-ray photo electron spectroscopic (XPS) analyses were conducted on a Thermo ESCALAB 250 analyser. An Al Kα X-ray source ($h\nu$ = 1486.6 eV) was operated with a pass energy of 30 eV. The photoluminescence (PL) measurement was performed on a LabRam confocal Raman microscope made by JY Company, excited by the 325 nm line of acontinuous He−Cd laser at room temperature.

2.3. Photocatalytic Activity Measurement. The evaluation of photocatalytic activity of the samples for the photocatalytic removal of Cr(VI) and MO in aqueous solution was performed at ambient temperature. $K_2Cr_2O_7$ was used as the sources of Cr(VI). The reaction suspension was prepared by adding 40 mg of photocatalyst powders into 80 mL of Cr(VI) solution (8 mg/L), MO solution (20 mg/L), or their mixture without the change of concentration. The pH value of the reaction suspension was adjusted to 4 using HCl or NaOH. Before irradiation, the suspensions were sonicated for 3 min and then magnetically stirred in dark conditions for 30 min to establish adsorption/desorption equilibrium. The suspension was then irradiated under UV light (300 W UV lamp) with a maximum emission at about 365 nm. After different irradiation intervals, 3.0 mL sample was taken from the reaction suspension and centrifuged to remove the photocatalyst powders for analysis. A spectrophotometer (CARY-5E) was used to record the UV−vis absorption spectra of the centrifuged solutions. The concentration of MO was determined by the absorption peaks at 464 nm. Changes in Cr(VI) concentration were followed by the spectrophotometric method of the diphenylcarbazide at 540 nm. The total Cr ions concentrations were measured by an inductively coupled plasma-optical emission spectrophotometer (ICP 6000 Thermal Electron). All the photocatalytic measurement mentioned were repeated twice to make sure the reliability of the results. The recycle ability of the NTMs was also tested. The catalyst after photocatalytic reaction was soaked in 10% HNO_3 solution for 5 h, then washed with deionized water and ethanol for several times and dried at 70 °C. The reborn NTMs catalyst was tested in the fresh mixture solution of Cr(VI) and MO under the same experimental conditions as mentioned above.

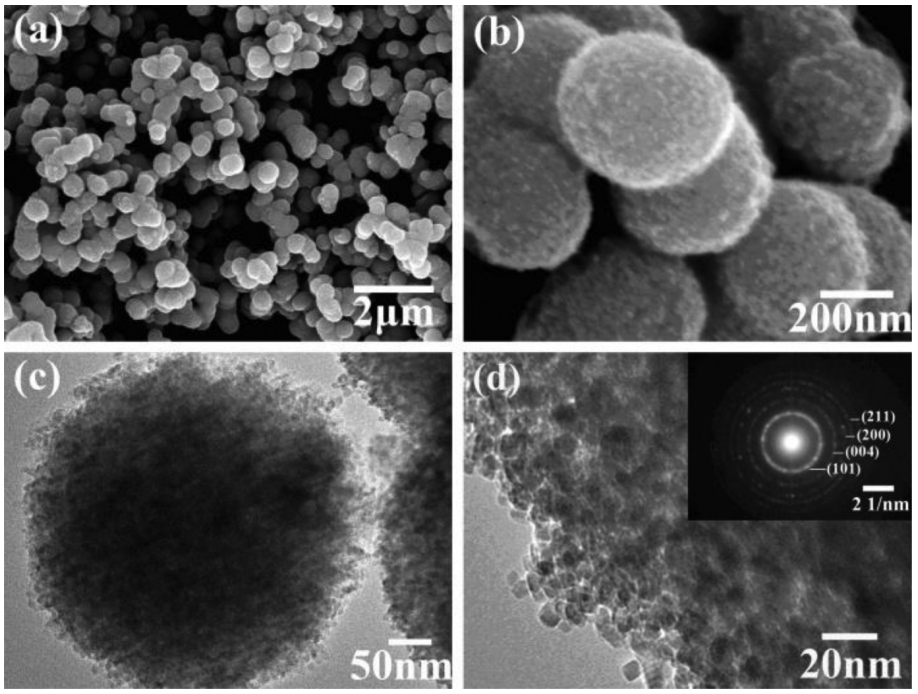

Figure 1. Morphological characteristics of NTMs: (a) the low-magnification FESEM image, (b) the enlarged FESEM image, (c) the TEM image, and (d) the high-magnification TEM image and SAED pattern (inset).

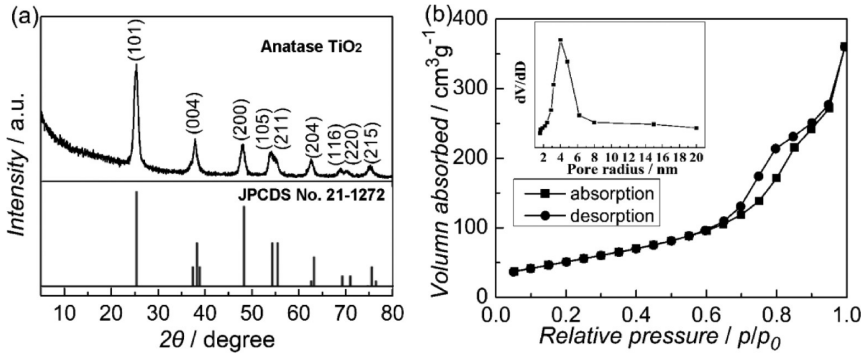

Figure 2. (a) XRD pattern and (b) nitrogen sorption isotherms of the NTMs (the inset shows the pore size distribution).

3. RESULTS AND DISCUSSION

3.1. Structural Characteristics. Figure 1a shows the low-magnification FESEM image of the large quantities of the as-synthesized NTMs with an average diameter ~0.5 μm. From the high-magnification FESEM image (Figure 1b), it can be seen that the surface of the spheres is rough. The TEM image (Figure 1c) further reveals a high density of channels/pores in a single microsphere. Figure 1d shows a typical high-magnification TEM image of the surface edge of a microsphere, confirming that the microsphere is composed of TiO_2 nanoparticles with an average size around 10 nm. Selected-area electron diffraction (SAED) pattern of the NTMs shows the polycrystalline diffraction rings corresponding to the indices of the lattice planes of the anatase phase TiO_2.[24] From the further high-magnification TEM images (see Figure S1 in Supporting Information), the crystal fringe of anatase TiO_2 (101) facets can be clearly seen, indicating that each small nanoparticle was a well-crystallized anatase phase TiO_2 single crystal.

The XRD pattern of the as-synthesized NTMs is given in Figure 2a. All peaks can be indexed as pure anatase phase of TiO_2 (JPCDS No. 21-1272). No impurity peak is observed. According to the Scherrer equation, the average crystallite size is ~9.4 nm, in good agreement with the TEM observation. To study the internal pore structures and specific surface area of the NTMs, the nitrogen adsorption-desorption measurement was carried out (Figure 2b). The obtained isotherm exhibits a type IV (Brunauer–Deming–Deming–Teller (BDDT) classification), revealing the existence of abundant mesoporous structures in the fabricated architectures.[25] On the basis of the BET equation, the obtained NTMs possess a specific surface area of 124 $m^2\ g^{-1}$, which is much higher than that of the micro/nanostructured TiO_2 reported.[26,27] The high specific surface area and abundant pores are of the necessities for a high performance photocatalyst.[26] The pore sizes distribution is found to centered around 4 nm (inset in Figure 2b).

3.2. Control Growth. The effect of microwave reaction temperature on the formation of NTMs was firstly investigated (Figure 3). It was found that all products were spherical shapes with uniform diameters around 0.5 μm, when the temperatures were changed from 120 to 160 °C (Figure 3a–3c). But the corresponding TEM images of the surface edge of the

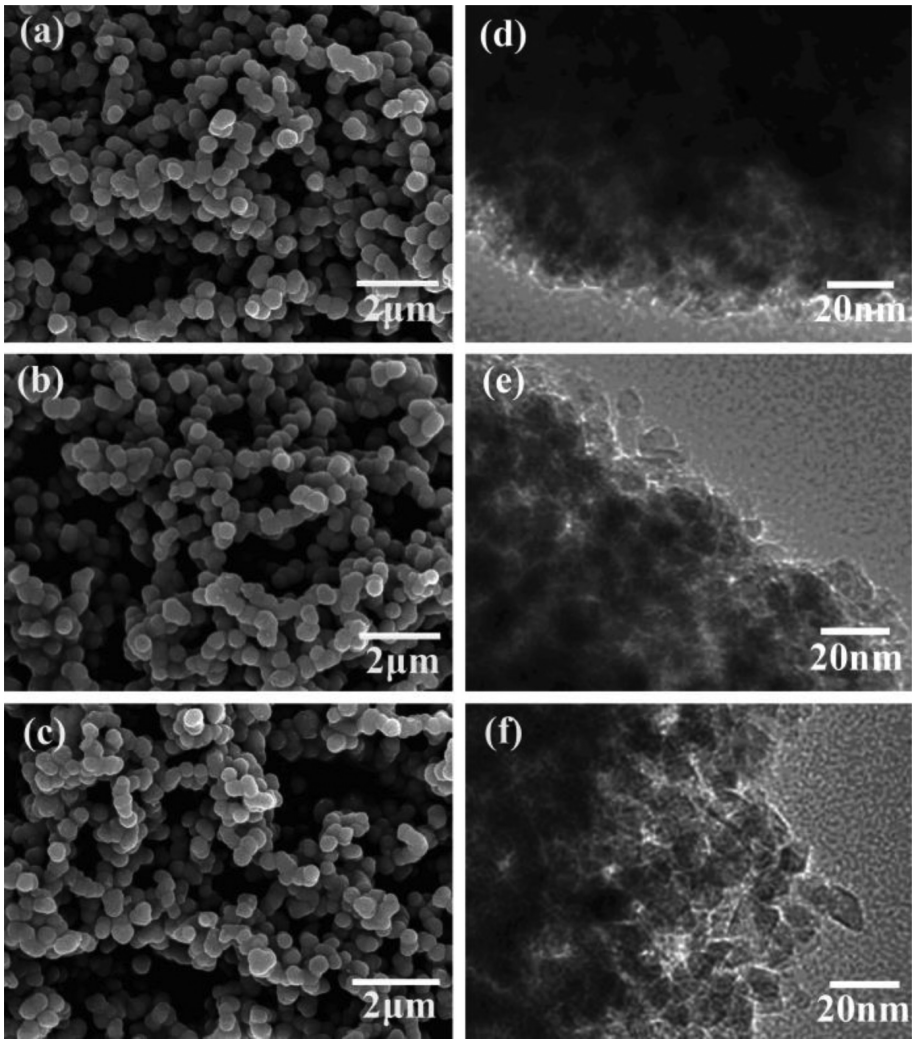

Figure 3. FESEM images of the products synthesized under the microwave radiation for 30 min with different temperatures: (a) 120 °C, (b) 140 °C, (c) 160 °C, and (d–f) corresponding TEM images.

microspheres (Figure 3d–3f) revealed that the interparticle pore sizes of the microspheres increased with the reaction temperatures increased from 120 to 160 °C, resulting from the increase of the nanoparticles sizes. All products can be indexed as pure anatase phase of TiO_2 in accordance with the XRD patterns (Figure S2a, Supporting Information). The average crystallite sizes of the resultant TiO_2 samples calculated from the broadening peak (101) of anatase phase according to the Scherrer Formula were 5.1, 8.8, and 9.2 nm when the reaction temperatures were increased from 120 to 140 and 160 °C, respectively. It is well known that the particle size and interparticle pore size are the key attributes in determining the surface area of the NTMs, strongly influencing the photocatalytic activity.[25,26] The above results indicate that such key attributes can be readily controlled by controlling the reaction temperature without changing the morphology of the microspheres.

The NTMs formation process was investigated. Figure S3 (see Supporting Information) shows the time-dependent morphological evolution under 180 °C. The spherical alike particle aggregates were rapidly formed during the initial stage of the reaction (e.g., 5 min). The surface of the aggregated particles was found to be smooth, implying a nonporous nature. The separation of the aggregated spherical particles occurred with prolonged reaction time (e.g., 10 min), signifying the beginning of NTMs formation. At this stage, the surface of the formed spheres became rough, implying the formation of nanoparticulate structures. When the reaction time was further increased to 20 min, nearly matured NTMs were formed. The matured NTMs with distinguished nanoparticulate structures were obtained after 30 min of reaction (Figure 1). All products can be indexed as pure anatase phase of TiO_2 according to the XRD patterns (Figure S2b, Supporting Information), and decrease of peak width at half height was observed with the prolonging of reaction time, indicated that the crystallization of the products increased.

The formation of NTMs can be described below. During the heating process, the formation of anatase TiO_2 nanoparticles might undergo the following reaction processes:[27]

Hydrolysis

$$Ti^{4+} + 4H_2O \rightarrow Ti(OH)_4 + 4H^+ \quad (1)$$

Condensation

$$Ti(OH)_4 \rightarrow TiO_2(\text{amorphous}) + 2H_2O \quad (2)$$

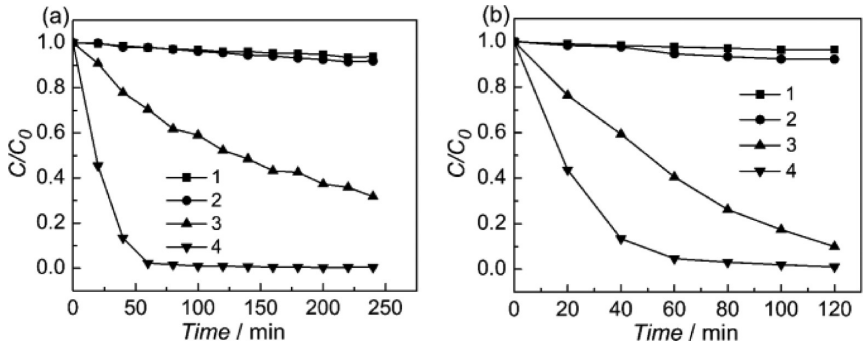

Figure 4. Conversion of (a) Cr(VI) and (b) MO. C_0 is the initial concentration of Cr(VI) or MO, C is concentration of the remaining Cr(VI) or MO at time t. Curves 1−4: Without photocatalyst in Cr(VI) or MO single system, without photocatalyst in the mixed system of Cr(VI) and MO, NTMs in the Cr(VI) or MO single system, and NTMs in the mixed system of Cr(VI) and MO, respectively.

Crystallization

$$TiO_2(\text{amorphous}) \rightarrow TiO_2(\text{anatase}) \quad (3)$$

Clearly, the reaction system pH is an important parameter affecting the hydrolysis and condensation reactions. The reaction 1 suggests that the hydrolysis reaction would be slower with acidic conditions and can be rapidly increased under alkaline conditions. In this work, urea was chosen to control the reaction system pH. When H_2SO_4 (1 M) was used to replace urea (0.1 M) while other experimental conditions were retained, only randomly dispersed nanoparticles could be produced (Figure S4a, Supporting Information). Under such strong acidic condition, the hydrolysis was greatly suppressed, leading to slow condensation nucleation processes. As a result, fewer metastable TiO_2 nanoclusters could be formed and the progressive crystal growth instead of particle aggregation into the microspheres dominated the formation process. Besides, the aggregation of metastable TiO_2 nanoclusters might be suppressed to a certain extent by the electrostatic repulsion, when considers their positively-charged surface status (the isoelectric point pH of TiO_2 is 5.5−6).[27] When ammonia (0.2 M) was employed to replace urea (0.1 M), random nanoparticles were observed (Figure S4b, Supporting Information), suggesting strong basic conditions were also unfavorable for formation of NTMs due to the excessively fast hydrolysis processes. These suggest that a suitable pH is critical for formation of NTMs. In this work, urea provides such needed conditions. Urea was decomposed to produce NH_3 under hydrothermal conditions, the slow releasing of OH^- would finely and in real-time controlled pH of the reaction system around 6.8, suitable for NTMs formation as such a pH value was closed to the isoelectric point pH of TiO_2.[27] This pH condition is favorable for metastable TiO_2 nanoparticles self-organized into microspheres.[27]

It should be noted that the fast formation of NTMs achieved in this work was due to the unique advantage of effective and efficient volumetric heating of the microwave method, that is, the temperature of the reaction mixture was raised uniformly throughout the whole liquid volume by direct coupling of microwave electromagnetic radiation energy to the water molecules presented in the reaction mixture.[28] As demonstrated, the microwave treatment is capable of greatly accelerating the reaction process and reducing the reaction time nearly an order of magnitude in comparison with the conventional hydrothermal method.[28,29] Also, homogeneous reaction conditions created by microwave lead to the formation of uniformly-sized NTMs, comparing to those of TiO_2 spheres prepared by the conventional electric oven hydrothermal method.[30]

3.3. Synergistic Photocatalytic Removal of Cr(VI) and MO. The photocatalytic activities of NTMs were evaluated by simultaneous photocatalytic decontamination of Cr(VI) and MO (a typical organic pollutant in the textile industry) under UV light irradiation. For comparison purpose, the photocatalytic decontamination of Cr(VI) and MO alone were conducted, Figure 4 shows the results. Blank experiments suggested that the concentration changes of Cr(VI) and MO resulting from the photolysis treatment under UV light irradiation without photocatalyst could be ignored, either in the single system or the mixed system of Cr(VI) and MO (curves 1 and 2 in Figure 4). Dark absorption of Cr(VI) and MO was also negligible (<10%), either in the single system or the mixed system of Cr(VI) and MO. It was worth mentioning that both the conversion rate of Cr(VI) and MO in the mixed system (curve 4 in Figure 4) was markedly faster than that in the Cr(VI) or MO single system (curve 3 in Figure 4). For instance, after 60 min of UV light irradiation, the Cr(VI) removal was 30% in the Cr(VI) single system (curve 3 in Figure 4a) and 98% in the mixed system (curve 4 in Figure 4a), respectively.

Comparative experiments under the same experimental conditions and procedures mentioned above were performed to investigate the photocatalytic activity of a commercially available TiO_2 photocatalysts, Degussa P25 (Figure S5, Supporting Information). Degussa P25 with the mixed anatase and rutile phases has been widely used as the benchmark photocatalyst for photocatalytic activity evaluations.[14,25,27] Within relatively low concentrations of Cr(VI) and MO, their photocatalytic process and reaction kinetics can be expressed by a pseudo-first-order reaction and apparent rate constant (k_{app}), respectively.[7,25] Table 1 shows the obtained k_{app} from NTMs and Degussa P25. For the single systems, Degussa P25 possess the highest k_{app} for both Cr(VI) and MO samples comparing to that of the NTMs. However, the photocatalytic activity of

Table 1. Reaction Rate Constant k_{app} (min^{-1}) in the Single (Cr(VI) or MO) or Mixed System (Cr(VI) and MO) with the Different TiO_2 Samples

	decontamination of Cr(VI)		decontamination of MO	
sample	single system	mixed system	single system	mixed system
NTMs	5.0×10^{-3}	5.8×10^{-2}	1.7×10^{-2}	5.0×10^{-2}
Degussa P25	1.0×10^{-2}	1.9×10^{-2}	6.1×10^{-2}	2.7×10^{-2}

NTMs surpasses Degussa P25 in the mixed system. For Degussa P25, the obtained k_{app} ratios of mixed and single systems for photocatalytic reduction of Cr(VI) and oxidation of MO are found to be 1.9 and 0.44, respectively, suggesting a positive synergistic effect for Cr(VI) reduction but a negative effect for MO oxidation in the mixed system. In strong contrast, the k_{app} ratios of 11.6 and 2.9 are obtained from NTMs for photocatalytic reduction of Cr(VI) and oxidation of MO. This confirms a highly significant synergistic effect in the simultaneous photocatalytic decontamination of Cr(VI) and MO with NTMs as the photocatalyst. Above results suggest that the synergistic effect is dependent of the structure of the photocatalysts.

The effect of Cr(VI) and MO concentrations on the simultaneous decontamination of Cr(VI) and MO using NTMs as photocatalyst was also studied (see Figure S6 and Figure S7 in Supporting Information), it was found that the Cr(VI) and MO concentrations did not have obvious effect on the synergistically enhanced phenomenon in the photocatalytic time 80 min. Both the Cr(VI) reduction and MO oxidation removal efficiencies were dramatically enhanced in the mixed system compared to that of single system with the different Cr(VI) and MO concentrations. This indicated that concentrations of Cr(VI) and MO did not influence the nature of NTMs and the synergistically enhanced removal activities of NTMs can be realized in a wide range of pollutants concentration.

The synergistic enhancement of photocatalytic reduction of Cr(VI) and oxidation of MO at NTMs for the mixed system is schematically illustrated in Figure 5. When Cr(VI) and MO are co-existed in a sample, on one hand, Cr(VI) as a strong oxidant is capable of rapidly consuming photocatalytically generated electrons at the conduction bend of NTMs to effectively suppress the charge recombination, while on the other hand, MO as an oxidisable organic matter consumes the photocatalytically generated holes at the valence band to further suppress the charge recombination. Such synergistic action by Cr(VI) and MO at the conduction and valence bands of NTMs can effectively and efficiently suppress the electron−hole recombination, leading to a dramatically enhanced photocatalytic efficiency when compared to the single systems.[4,11−13] It is well known that the rutile conduction band edge potential is ~0.2 V more positive than that of the anatase, providing a driving force for charge separation.[31,32] The PL spectrum measurements have been widely used to express the charge recombination behavior of the semiconductor material.[33−36]

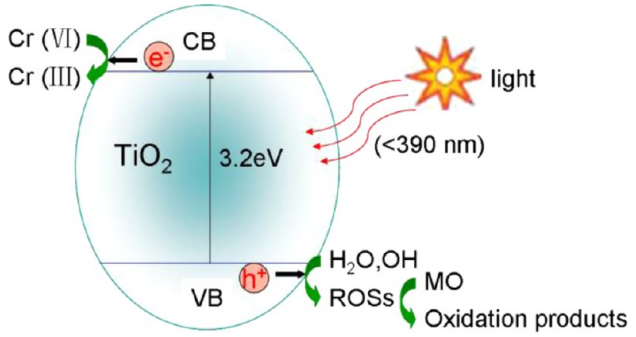

Figure 5. Schematic illustration of the mechanism of the simultaneous decontamination of Cr(VI) and MO by NTMs under UV light irradiation, ROSs represents reactive oxidative species.

Figure S8 (see Supporting Information) shows the PL spectra of NTMs and Degussa P25 samples measured under an excitation wavelength of 325 nm at room temperature. As the PL signal can be assigned to the radiative recombination of self-trapped exciton, the stronger the PL signal, the stronger the recombination of photocatalytically generated electrons and holes.[35] Degussa P25 exhibits a much weaker PL signal comparing to NTMs, implying a lower rate of charge recombination than that of NTMs, the superior charge separation ability of Degussa P25 induced by the mixed anatase and rutile phases can explain its excellent photocatalytic activity in Cr(VI) or MO single system. In this work, the enhanced photocatalytic efficiency in Cr(VI) and MO mixed system compared to that of single system is mainly due to the enhanced charge separation effect. The less significant synergistic effect observed for Degussa P25 could be largely attributed to its superior charge separation ability induced by the mixed anatase and rutile phases.[31,32] Under the circumstance, the mixing of Cr(VI) and MO contributes little to further improve the charge separation in Degussa P25, hence, less significant synergistic effect can be observed in the simultaneous photocatalytic decontamination of Cr(VI) and MO. Therefore, the intrinsic catalytic performance of Degussa P25 is not effective for the simultaneous treatment of Cr(VI) and MO. In contrast, NTMs showed relative lower photocatalytic efficiency in Cr(VI) or MO single system compared to Degussa P25 because of its single anatase phase, which was not benefit for the charge separation, however, it showed great potential in the simultaneous photocatalytic decontamination of Cr(VI) and MO. Moreover, the hierarchical mesoporous structures of NTMs would induce better harvesting and multiple reflecting of light,[25] further promote the synergistic effect, leading to the enhanced photocatalytic efficiency in the mixed system. The strong synergistic photocatalytic activity of NTMs might be also ascribed to the structure-induced enhancement of photocatalytic performance of micro/nanostructure.[14−16]

It should be mentioned that the catalyst may become deactivated to some extent due to the formation of precipitates and complexes (e.g., surface-absorbed Cr or organic species) at the catalyst surface that block the active sites of the catalyst in the mixed system, which hinders the further photocatalytic reaction.[3] The catalyst deactivation might be another reason for that the synergistic photocatalytic effect could not be realized using Degussa P25,[3] when considering its relative lower specific surface area (50 m^2 g^{-1}) compared to NTMs, which would be further reduced during liquid phase photocatalysis due to the easy aggregation property of the nano-sized structure. In contrast, the high specific surface area and abundant mesoporous structure of NTMs can provide ideal channels for easy and fast diffusion of the Cr(VI) and MO molecules to contact the TiO_2 nanoparticles,[15] and the effective against agglomeration feature of micro/nanostructure may hinder the further reduction of the specific surface area of NTMs during liquid phase photocatalysis. In this regard, the unique morphological structures of NTMs (e.g., high specific surface area and abundant mesoporous structures) equip the catalyst with high tolerance toward the surface deactivation.

To further understand the photocatalysis process, the total residual Cr ions concentrations in NTMs photocatalytic after treated samples were measured by ICP emission spectrometer (Figure S9, Supporting Information). For the single system after 240 min treatment, a 1.8 ppm of total residual Cr ions

concentration was measured. However, for the mixed system after a shorter treatment time of 80 min, the measured total residual Cr ions concentration was found to be as low as 0.034 ppm, much lower than the maximum allowable Cr(VI) concentrations of 0.25 ppm for industrial wastewater and 0.05 ppm for drinking water.[6]

XPS was used to further study the surface absorbing Cr of the NTMs after photocatalytic reaction in the single and mixed systems (Figure S10, Supporting Information). The broad peak of Cr $2p^{3/2}$ could be fitted to several peaks at different binding energies. Three main peaks centered at 576.3, 576.5, and 577.6 eV are consistent with the published XPS spectra characteristics of oxides or the hydroxide forms of Cr(III) (e.g., $Cr(III)_xO_y$ and $Cr(OH)_3$), the other two subordinate peaks at 579.6 and 580.3 eV are corresponded to the characteristics binding energy for the adsorbed Cr(VI).[37,38] The presence of oxide or hydroxide forms of Cr(III) confirms the photocatalytic reduction of Cr(VI). The result also confirms that the synergistic photocatalysis at NTMs is not only capable of simultaneously reducing Cr(VI) and oxidizing MO, but also has the capability to remove Cr ions via adsorption.

The recovery of photocatalysts after use is of a critical practical issuel.[39] In the present study, we found that the NTMs could be readily separated from water via a facile sedimentation process in less than 1 h, while the aqueous suspensions of Degussa P25 powder were still turbid after several hours (Figure S11, Supporting Information). The easy recovery feature make possible to reuse the NTMs. Figure 6 shows the

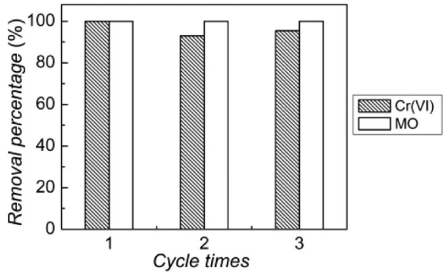

Figure 6. Cr(VI) and MO removal performance in three cycles for the NTMs.

performance of the recycled NTMs for the mixed system of Cr(VI) and MO (60 min of UV light irradiation for each cycle). The recycled NTMs were treated by HNO_3 solution before used to remove the surface-absorbed Cr species.[39] It was found that the Cr(VI) removal efficiency of NTMs was still up to 95.5% after three cycles, while the removal efficiency of MO maintained 100%. These results demonstrate a feasibility of recovery and reuse of NTMs.

4. CONCLUSIONS

We have demonstrated a facile and high yield microwave-assisted hydrothermal method to fabricate uniformly sized NTMs constructed with well-crystallized anatase phase nanoparticles. The reaction time could be dramatically reduced to 30 min, an order of magnitude shorter than that of conventional hydrothermal methods, due to the rapid heating capability of microwave. The fabricated NTMs were highly uniform in size, having an average diameter of ~0.5 μm, resulting from the uniform microwave heating capability. The resultant NTMs were constructed by well-crystallized anatase phase nanoparticles ranging from 5 to 10 nm, possess abundant mesoporous structures with a high specific surface area of 124 $m^2\ g^{-1}$. The formation of NTMs could be through an in situ self-aggregation process under controllable pH in presence of urea. At present, it still has rarely previous reports about this innovative approach to synthesize the micro/nanostructured TiO_2. The application of NTMs for simultaneous photocatalytic decontamination of Cr(VI) and MO demonstrated a strong synergistic effect that dramatically enhanced both Cr(VI) reduction and MO oxidation removal efficiencies, showing great potential in detoxification of harmful pollutants in wastewaters. Regeneration studies showed the feasibility of regeneration of NTMs. This work not only enriched the synthesis methods of the micro/nanostructured TiO_2, but also provided a new means to improve the photocatalytic efficiency via structural-induced synergistic effect, applicable to the other catalysis systems.

■ ASSOCIATED CONTENT

Supporting Information

HRTEM images of NTMs with the different magnification, XRD patterns of the products prepared with the different reaction temperature and reaction time, FESEM images of the as-synthesized products at 180 °C with the different reaction times, FESEM images of the TiO_2 synthesized at 180 °C for 30 min with 1 M H_2SO_4 and 0.2 M ammonia, conversion of MO and Cr(VI) with Degussa P25 as photocatalyst, FESEM image of Degussa P25 powders, effect of Cr(VI) and MO concentrations on the simultaneous decontamination of Cr(VI) and MO using NTMs as the photocatalyst, photoluminescence spectra of the different TiO_2 powders, concentrations of the total residual Cr ions in the photocatalytic reaction solutions with NTMs as photocatalysts under UV light irradiation, XPS spectra of the NTMs powders after photocatalytic reaction, and appearance of suspensions containing two different types of photocatalysts in water after 1 h. This information is available free of charge via the Internet at http://pubs.acs.org/.

■ AUTHOR INFORMATION

Corresponding Author

*E-mail: gzhwang@issp.ac.cn.

Author Contributions

The manuscript was written through contributions of all authors. All authors have given approval to the final version of the manuscript.

Notes

The authors declare no competing financial interest.

■ ACKNOWLEDGMENTS

This work was supported by the National Basic Research Program of China (Grant No. 2013CB934302), the Natural Science Foundation of China (Grant No. 51072199), and Strategic Priority Research Program of the Chinese Academy of Sciences (Grant No. XDA09030200).

■ REFERENCES

(1) Cappelletti, G.; Bianchi, C. L.; Ardizzone, S. *Appl. Catal., B: Environ.* **2008**, *78*, 193−201.

(2) Meichtry, J. M.; Brusa, M.; Mailhot, G.; Grela, M. A.; Litter, M. I. *Appl. Catal., B: Environ.* **2007**, *71*, 101−107.

(3) Papadam, T.; Xekoukoulotakis, N. P.; Poulios, I.; Mantzavinos, D. *J. Photochem. Photobiol., A: Chem.* **2007**, *186*, 308−315.

(4) Schrank, S. G.; Jose, H. J.; Moreira, R. F. P. M. *J. Photochem. Photobiol., A: Chem.* **2002**, *147*, 71−76.

(5) Lee, S. M.; Lee, T. W.; Choi, B. J.; Yang, J. K. *J. Environ. Sci. Health, Part A: Toxic/Hazard. Subst. Environ. Eng.* **2003**, *38*, 2219−2228.
(6) Fan, J. W.; Liu, X. H.; Zhang, J. *Environ. Technol.* **2011**, *32*, 427−437.
(7) Yang, J. K.; Lee, S. M.; Farrokhi, M.; Giahi, O.; Siboni, M. S. *Desalin. Water Treat.* **2012**, *46*, 375−380.
(8) Li, J. Q.; Wang, D. F.; Liu, H. I.; He, Z. L.; Zhu, Z. F. *Appl. Surf. Sci.* **2011**, *257*, 5879−5884.
(9) Yu, J. G.; Xiang, Q. J.; Ran, J. R.; Mann, S. *CrystEngComm* **2010**, *12*, 872−879.
(10) Liu, M.; Lv, K. L.; Wang, G. H.; Wang, Z. Y.; Zhao, Y. X.; Deng, Y. R. *Chem. Eng. Technol.* **2010**, *33*, 1531−1536.
(11) Kyung, H.; Lee, J.; Choi, W. Y. *Environ. Sci. Technol.* **2005**, *39*, 2376−2382.
(12) Dozzi, M. V.; Saccomanni, A.; Selli, E. *J. Hazard. Mater.* **2012**, *211*, 188−195.
(13) Wang, Q.; Chen, X. S.; Yu, K.; Zhang, Y.; Cong, Y. Q. *J. Hazard. Mater.* **2013**, *246*, 135−144.
(14) Lu, F.; Cai, W. P.; Zhang, Y. G. *Adv. Funct. Mater.* **2008**, *18*, 1047−1056.
(15) Duan, X. W.; Wang, G. Z.; Wang, H. Q.; Wang, Y. Q.; Shen, C.; Cai, W. P. *CrystEngComm* **2010**, *12*, 2821−2825.
(16) Li, J.; Wang, G. Z.; Wang, H. Q.; Tang, C. J.; Wang, Y. Q.; Liang, C. H.; Cai, W. P.; Zhang, L. D. *J. Mater. Chem.* **2009**, *19*, 2253−2258.
(17) Yu, J. G.; Liu, W.; Yu, H. G. *Cryst. Growth Des.* **2008**, *8*, 930−934.
(18) Li, X. X.; Xiong, Y. J.; Li, Z. Q.; Xie, Y. *Inorg. Chem. Commun.* **2006**, *45*, 3943−3945.
(19) Yang, W. G.; Wan, F. R.; Chen, Q. W; Li, J. J.; Xu, D. S. *J. Mater. Chem.* **2010**, *20*, 2870−2876.
(20) Sun, Z. Q.; Kim, J. H.; Zhao, Y.; Bijarbooneh, F.; Malgras, V.; Lee, Y.; Kang, Y. M.; Dou, S. Y. *J. Am. Chem. Soc.* **2011**, *133*, 19314−19317.
(21) Chen, J. S.; Tan, Y. L.; Li, C. M.; Cheah, Y. L.; Luan, D. Y.; Madhavi, S.; Boey, F. Y. C.; Archer, L. A.; Lou, X. W. *J. Am. Chem. Soc.* **2010**, *132*, 11914−11916.
(22) Xiang, Q. J.; Yu, J. G.; Cheng, B.; Ong, H. C. *Chem. Asian J.* **2010**, *5*, 1466−1474.
(23) Yu, J. G.; Zhang, J. *Dalton Trans.* **2010**, *39*, 5860−5867.
(24) Han, C.; Luque, R.; Dionysiou, D. D. *Chem. Commun.* **2012**, *48*, 1860−1863.
(25) Yu, J. G.; Shi, L. *J. Mol. Catal. A: Chem.* **2010**, *326*, 8−14.
(26) He, Z. L.; Zhu, Z. F.; Li, J. Q.; Zhou, J. Q.; Wei, N. *J. Hazard. Mater.* **2011**, *190*, 133−139.
(27) Liu, S. W.; Yu, J. G.; Mann, S. *Nanotechnology* **2009**, *20*, 325606−325613.
(28) Pol, V. G.; Langzam, Y.; Zaban, A. *Langmuir* **2007**, *23*, 11211−11216.
(29) Baghbanzadeh, M.; Carbone, L.; Cozzoli, P. D.; Kappe, C. O. *Angew. Chem., Int. Ed.* **2011**, *50*, 2−50.
(30) Zhou, M. H.; Xu, J.; Yu, H. G.; Liu, S. W. *J. Phys. Chem. Solids* **2010**, *71*, 507−510.
(31) Jiang, D.; Zhang, S.; Zhao, H. *J. Catal.* **2007**, *250*, 103−110.
(32) Jiang, D.; Zhang, S.; Zhao, H. *Environ. Sci. Technol.* **2007**, *41*, 303−308.
(33) Su, C. Y.; Liu, L.; Zhang, M. Y.; Zhang, Y.; Shao, C. L. *CrystEngComm* **2012**, *14*, 3989−3999.
(34) Etacheri, V.; Seery, M. K.; Hinder, S. J.; Pillai, S. C. *Chem. Mater.* **2010**, *22*, 3843−3853.
(35) Jing, L. Q.; Qu, Y. C.; Wang, B. Q.; Li, S. D.; Jiang, B. J.; Yang, L. B.; Fu, W.; Fu, H. G.; Sun, J. Z. *Sol. Energy Mater. Sol. Cells* **2006**, *90*, 1773−1787.
(36) Fujihara, K.; Izumi, S.; Ohno, T.; Matsumura, M. *J. Photochem. Photobiol. A: Chem.* **2000**, *132*, 99−104.
(37) Mullet, M.; Demoisson, F.; Humbert, B.; Michot, L. J.; Vantelon, D. *Geochim. Cosmochim. Acta* **2007**, *71*, 3257−3271.
(38) Shuttleworth, D. *J. Phys. Chem.* **1980**, *84*, 1629−1634.
(39) Xu, S. C.; Zhang, Y. X.; Pan, S. S.; Ding, H. L.; Li, G. H. *J. Hazard. Mater.* **2011**, *196*, 29−35.